Bulletin of the Seismological Society of America. Vol. 67, No. 3, pp. 929–956. June 1977

EFFECTS OF CROSS-AXIS SENSITIVITY AND MISALIGNMENT ON THE RESPONSE OF MECHANICAL-OPTICAL ACCELEROGRAPHS

By H. L. Wong and M. D. Trifunac

ABSTRACT

Recorded strong-motion accelerograms may be affected by cross-axis sensitivity and the misalignment of their transducer sensitivity axes. The cross-axis sensitivity arises from the fact that the transducer mass when deflected from its ideal equilibrium position may experience additional deflection caused by the inertial forces perpendicular to the transducer's principal sensitivity axis. The misalignment effects result from imperfect positioning of transducers into the instrument housing so that the nominal sensitivity directions are not mutually perpendicular and/or do not coincide with the orthogonal reference frame attached to the instrument housing. If the misalignment effects cannot be accounted for, the recorded accelerations can be distorted by an amount, which for large input accelerations, may exceed the digitization noise level by as much as one order of magnitude.

In this paper a method is presented for a complete dynamic correction procedure which can eliminate any cross-axis and misalignment effects and yield exact accelerations for a reference coordinate system conveniently attached to the instrument housing. To carry out these correction procedures it is necessary to know the precise orientations of all transducers relative to the selected reference frame. A simple sequence of static tilt tests is proposed which provides adequate information for computation of all misalignment angles and estimation of transducer sensitivity constants.

Introduction

Accurate measurements of strong earthquake ground motion require advanced data analysis techniques and optimization of not only the recording hardware components but of the complete data acquisition system including the data processing methods. In developing such a system, care should be taken to balance all the sources of noise and hardware characteristics with the available methods for data reduction and subsequent analysis. For optical-mechanical accelerographs, for example, data analysis techniques have recently been summarized for use in routine engineering applications (Trifunac and Lee, 1973). These procedures incorporate corrections for transducer amplitude and phase distortions (Trifunac, 1972), for baseline detrending (Trifunac, 1971), and for numerous other factors which are either known or can be characterized in terms of nominal transducer properties (Trifunac *et al.*, 1973). However, throughout the development of these routine processing methods the possible influence of cross-axis sensitivity and transducer misalignment (Trifunac and Hudson, 1970) has been neglected. Even though these effects may be important under certain conditions, the correction for them requires systematic tilt tests which are not available for strong-motion data recorded so far.

A considerable amount of work has been done by numerous investigators to formulate the general equations of motion for hinged or similar type transducers subjected to translational and rotational support motion (e.g., Anderson and Wood, 1925;

Byerly, 1953; Benioff, 1955). The significance of selected wave types which lead to well-defined predominant motions in one or two directions has also been explored (Rodgers, 1968). Analysis and application of most of these results, however, was focused mainly on seismological studies. In 1973, Skinner and Stephenson presented a primarily static analysis of sensing direction errors and cross-axis interaction errors. They included a brief discussion of dynamic errors that, for the first time, dealt with strong-motion accelerographs. In 1975, Rogers examined the nonlinear response of pendulous accelerometers and considered the problems of cross-axis sensitivity.

The purpose of this paper is to extend this work and to present an analysis of cross-axis and misalignment effects for transient and arbitrary translational strong ground shaking. Although it is recognized that some rotational motion accompanies strong ground shaking, proper consideration of these rotational effects is well beyond the scope of this paper because three mutually perpendicular transducers are not capable of specifying all six components of motion at a point. Thus, in the analysis which follows, we will assume that the instrument base is subject to translational shaking only.

It can be shown that the spectral contribution by rotational (rocking) components of ground motion to the response of typical accelerograph transducers supported at a height h above the instrument base is approximately equal to $2\pi h/\lambda$ times the spectral amplitudes of translational motions, where λ represents the wavelength of incident waves. Since h is typically of the order of 10^0 to 10^1 cm, while λ is in the range 10^3 to 10^5 cm, it is seen that for the frequencies which are of interest in earthquake engineering and strong-motion seismology (say 0.1 to 25 Hz) this effect only rarely contributes up to about 1 per cent of translational spectral amplitudes.

One of the motivations for carrying out this study results from a desire to complete the final steps in a more complete set of procedures for routine data processing and analysis (Trifunac and Lee, 1973). Simple tilt tests followed by the routines for the elimination of cross-axis and misalignment effects should enable one to arrive at high quality digital accelerograms when starting from the final output of Volume II corrected data (Trifunac and Lee, 1973). This, of course, does not mean that all accelerograms will have to be processed to eliminate cross-axis and misalignment effects. These effects tend to become noticeable only for large accelerations and in most cases may be neglected for lower amplitude and longer period motions. Furthermore, the uncertainties associated with the orientation of the instrument housing may often be larger and in the end may produce distortions in the final results which exceed the contribution from the cross-axis and misalignment effects. Nevertheless, for those studies where special and detailed attention is required to extract fine details of the recorded motions, and especially when accurate estimates of the motions in mutually perpendicular directions are needed, these additional corrections can and should be performed.

Configuration of a Typical Strong-Motion Accelerograph

Figure 1 shows the top view of a typical general purpose strong-motion accelerograph which is designed to record strong ground shaking and structural response. This instrument records on a 70-mm film whose nominal speed is 1.0 cm/sec. It has two timing traces with a nominal timer accuracy better than 0.5 per cent. One of the timing traces can be connected with a WWVB radio receiver for recording absolute time on film when this instrument is used in the Continental United States (Dielman *et al.*,

1975). In the stand-by condition the current drawn by the vertical electromagnetic starter is about 0.15 mA. The standard 12-volt power supply consists of two rechargeable batteries which are drained by about 1-A current when the instrument is in full operation.

The mechanical transducer representing a single degree-of-freedom viscously damped oscillator is shown in Figure 2. The transducer mass cantilevered on two leaf springs consists of a plastic plate which supports a coil moving in a magnetic field. Typical coil resistance is about 25 Ω and a shunt resistor of approximately 10 Ω provides nominal damping of 0.6 ± 0.05 of critical. The optical system consists of two mirrors simi-

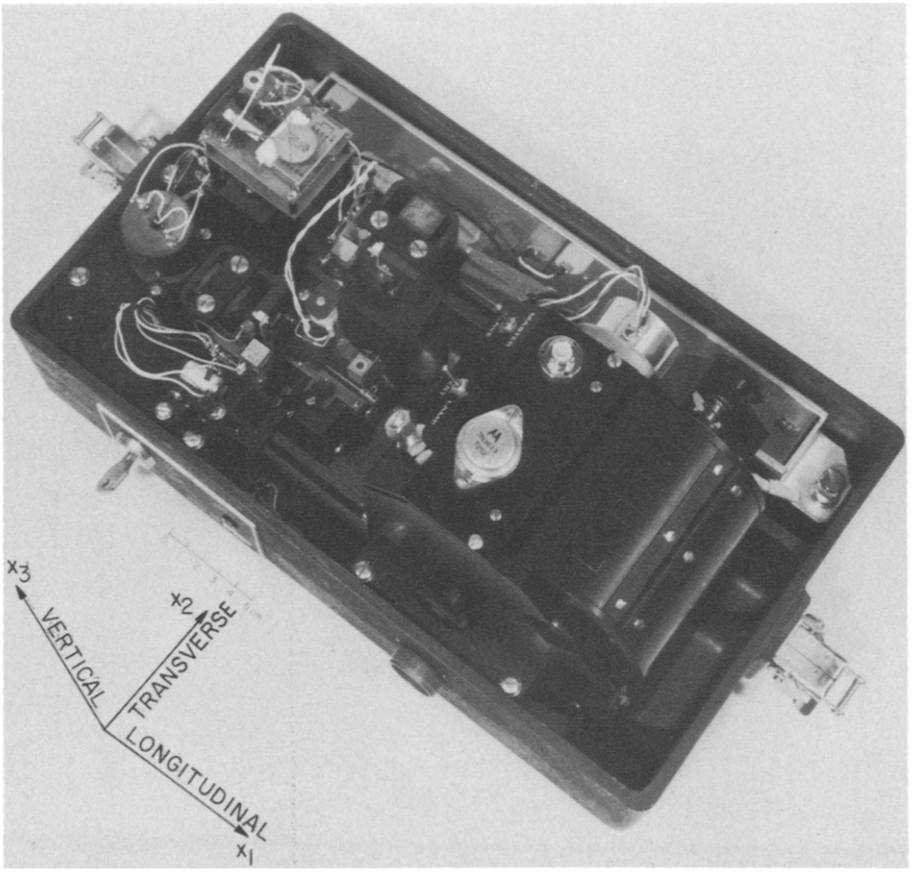

FIG. 1. Top view of Kinemetrics (SMA-1) strong-motion accelerograph.

lar to those used for the Wood-Anderson seismometer (Anderson and Wood, 1925). The light beam from a fixed source is first reflected off the transducer mirror toward the fixed mirror and then back toward the moving mirror. Upon the second reflection off the moving mirror the light beam is projected onto the film (Figure 2). This double mirror configuration results in the rotation of the undeflected beam of light by 4α when the moving mirror attached to the transducer is rotated by α. Such optical magnification permits the design of stiff leaf springs and with the length of the deflecting optical path equal to 125 mm leads to a convenient overall sensitivity of about 1.8 cm/g and a compact instrument housing. The natural frequency of such a transducer is about 25 Hz.

When installed in the field the orientation of an accelerograph is typically specified by the geographic directions in which its transverse and longitudinal axes point. For the purpose of this analysis, it will be assumed that these directions are accurately known and coincide with a set of orthogonal axes x_1, x_2, and x_3 as shown in Figure 1. Although it is convenient to select (x_1, x_2, x_3) coordinates to coincide with the longitudinal, transverse, and vertical axes of the instrument housing, it should be noted that the choice of such a reference coordinate system is quite arbitrary. The effects caused by the misalignment of transverse, longitudinal, and vertical transducers result from the fact that their sensitivity vectors are not mutually perpendicular and not from the fact that the coordinate system defined by these vectors does not coin-

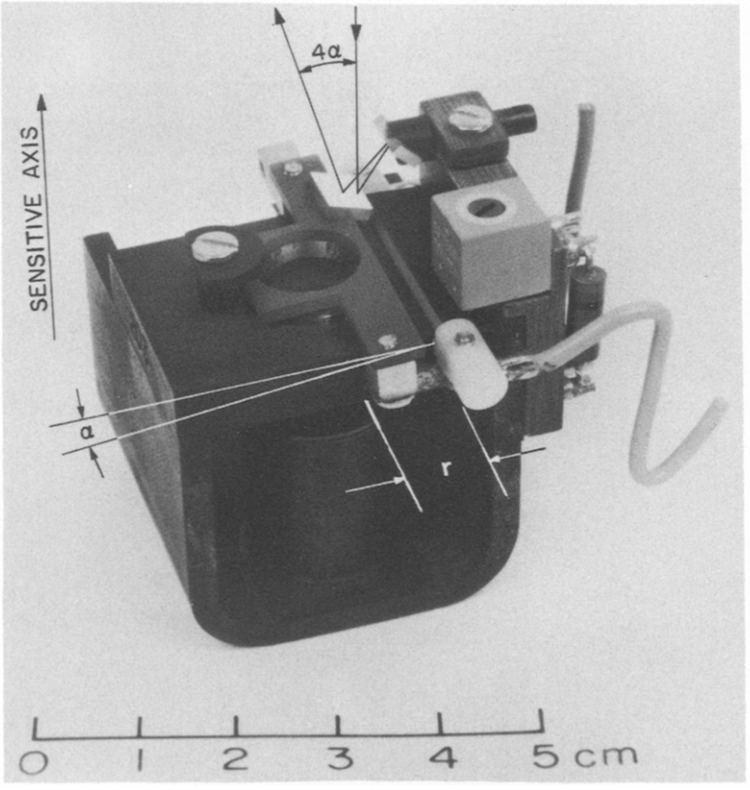

FIG. 2. A Kinemetrics (SMA-1) transducer.

cide with the longitudinal, transverse, and vertical axes of the instrument housing. In the MO-2 accelerograph, for example, the two horizontal sensitivity vectors are at 45° with respect to the longitudinal and transverse axes of the instrument housing (Skinner and Stephenson, 1973). For the accelerograph shown in Figure 1, the nominal sensitivity vectors should coincide with x_1, x_2, and x_3. For simplicity, the misalignment of the transducer masses relative to their ideal static positions on the x_1, x_2, and x_3 axes will be described by the angles φ_i, θ_i, and ψ_i for $i = 1, 2, 3$ (Figure 3).

For a transducer to be perfectly aligned in its static position one of the three mutually perpendicular axes (x_1^{pi}, x_2^{pi}, x_3^{pi}) must go through the fixed points of its two leaf springs (Figure 2), and the center of the transducer mass must lie on the second axis. The third axis, perpendicular to the previous two, must coincide with the direction of the tangent to the infinitesimal arc traced by the center of the transducer

mass for a small deflection off static equilibrium. The position of three coordinate systems (x_1^{pi}, x_2^{pi}, x_3^{pi}) for $i = 1, 2, 3$, in which the pendulums $i = 1, 2, 3$ are perfectly aligned, relative to the reference frame (x_1, x_2, x_3) (Figure 1) is specified by the nine angles φ_i, θ_i, ψ_i, for $i = 1, 2, 3$ which are shown in Figure 3.

The Effect of Cross-Axis Sensitivity

We consider an idealized pendulum with its sensitive axis directed along the x_1^{p1}-axis as shown in Figure 4a. The small deflection angle α_1 from static equilibrium is defined as positive when deflected by the positive acceleration $\ddot{x}_1^{p1}$. (In the following analysis, we shall frequently refer to a particular pendulum by the direction of its

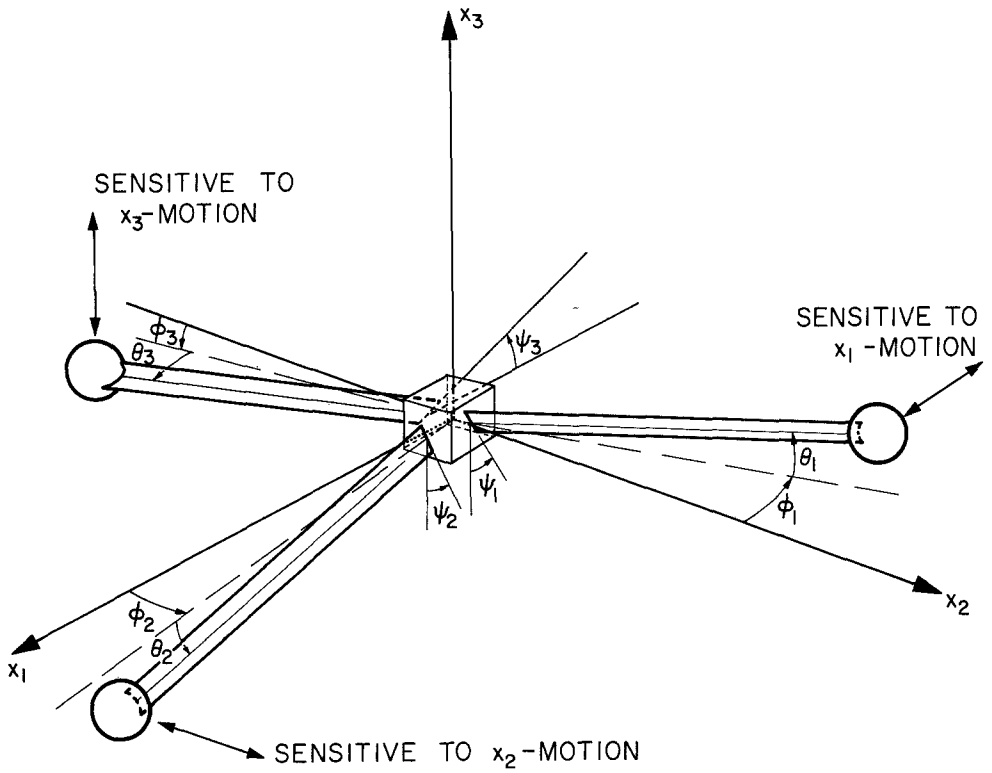

Fig. 3. Misalignment angles of the three transducers with respect to their ideal positions along x_1, x_2, and x_3 axes where $\varphi_i = \theta_i = \psi_i = 0$, $i = 1, 2, 3$, would be zero.

sensitive axis, e.g., the pendulum with its sensitive axis lying mainly in the direction of x_1 shall be called the "x_1-pendulum", etc.) The equation of motion for the x_1-pendulum may be obtained by the balance of moments about the pendulum pivot (Figure 4a), and is

$$m_1 r_1^2 \ddot{\alpha}_1 + c_1 r_1 \dot{\alpha}_1 + k_1 r_1 \alpha_1 = (m_1 \ddot{x}_1^{p1}) r_1 \cos \alpha_1 + (m_1 \ddot{x}_2^{p1}) r_1 \sin \alpha_1 \qquad (1)$$

where m_1, c_1, k_1, and r_1 are the mass, damping constant, stiffness constant, and the length of the arm of the x_1-pendulum, respectively. Dividing equation (1) by $m_1 r_1^2$ and rearranging gives

$$\ddot{\alpha}_1 + 2\omega_{n1} \zeta_1 \dot{\alpha}_1 + \omega_{n1}^2 \alpha_1 = \frac{1}{r_1} [\ddot{x}_1^{p1} \cos \alpha_1 + \ddot{x}_2^{p1} \sin \alpha_1], \qquad (2)$$

where ω_{n1} is the undamped natural frequency and ζ_1 is the fraction of critical damping for the x_1-pendulum. Equation (2) represents a differential equation for the deflection angle α_1, and it depends on both the $\ddot{x}_1^{p1}$ and $\ddot{x}_2^{p1}$ components of accelerations. Equation (1) is valid only when the center of gravity of the pendulum mass is far from the pivot point so that the distance r_1 becomes equal to the radius of gyration. For the transducer shown in Figure 2, for example, this is not true but the derived form of equation (2) remains the same provided r_1 in it is replaced to represent the ratio of the radius of gyration squared and the distance between the pivot point and the center of gravity of the transducer mass.

Generally, for a pendulum with a relatively stiff spring, the deflection α_1 per unit acceleration is small so that $\sin \alpha_1 \approx \alpha_1$ and $\cos \alpha_1 \approx 1$; hence, the contribution to the

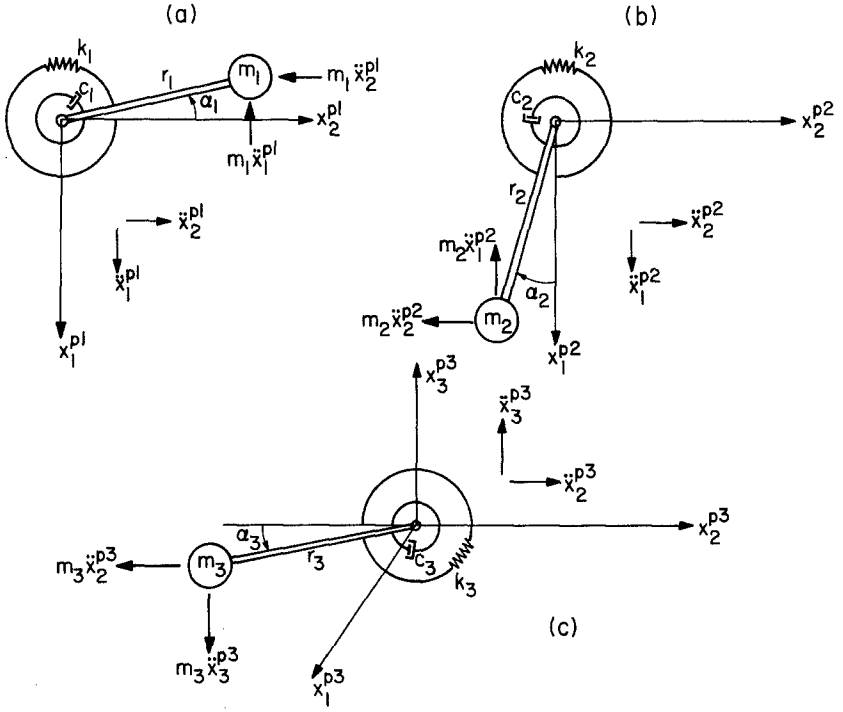

FIG. 4. Relative positions of the longitudinal (a), transverse (b), and vertical (c) pendulums in their respective x_1^{pi}, x_2^{pi}, x_3^{pi}, $i = 1, 2, 3$, reference frames.

response from $\ddot{x}_2^{p1}$ (frequently referred to as the "cross-axis" acceleration) is small compared to $\ddot{x}_1^{p1}$ for the x_1-pendulum. The possible effect of this cross-axis sensitivity, however, depends on the previous acceleration and on the simultaneous values of the orthogonal components $\ddot{x}_1^{p1}$ and $\ddot{x}_2^{p1}$. These effects will be illustrated later by numerical examples based on actual accelerograms.

The equations of motion for the x_2- and x_3-pendulums shown in Figure 4, b and c, are

$$\ddot{\alpha}_2 + 2\omega_{n2}\zeta_2\dot{\alpha}_2 + \omega_{n2}^2\alpha_2 = \frac{1}{r_2}[\ddot{x}_1^{p2}\sin\alpha_2 + \ddot{x}_2^{p2}\cos\alpha_2], \tag{3}$$

$$\ddot{\alpha}_3 + 2\omega_{n3}\zeta_3\dot{\alpha}_3 + \omega_{n3}^2\alpha_3 = \frac{1}{r_3}[\ddot{x}_3^{p3}\cos\alpha_3 - \ddot{x}_2^{p3}\sin\alpha_3]. \tag{4}$$

An accelerograph records the response of three pendulums: α_1, α_2, α_3 on film or paper for input accelerations $\ddot{\mathbf{x}}^{pi} = (\ddot{x}_1^{pi}, \ddot{x}_2^{pi}, \ddot{x}_3^{pi})$, $i = 1, 2, 3$. In the ideal case when the sensitive axes of these three pendulums are orthogonal to each other, the three sets of coordinates $\mathbf{x}^{p1}$, $\mathbf{x}^{p2}$, $\mathbf{x}^{p3}$ coincide, and equations (2), (3), and (4) may be combined to yield a linear matrix equation for the three components of $\ddot{\mathbf{x}}^p$

$$\begin{bmatrix} \cos\alpha_r & \sin\alpha_1 & 0 \\ \sin\alpha_2 & \cos\alpha_2 & 0 \\ 0 & -\sin\alpha_3 & \cos\alpha_3 \end{bmatrix} \begin{bmatrix} \ddot{x}_1^p \\ \ddot{x}_2^p \\ \ddot{x}_3^p \end{bmatrix} = \begin{bmatrix} r_r(\ddot{\alpha}_1 + 2\omega_{n1}\zeta_1\dot{\alpha}_1 + \omega_{n1}^2\alpha_1) \\ r_2(\ddot{\alpha}_2 + 2\omega_{n2}\zeta_2\dot{\alpha}_2 + \omega_{n2}^2\alpha_2) \\ r_3(\ddot{\alpha}_3 + 2\omega_{n3}\zeta_3\dot{\alpha}_3 + \omega_{n3}^2\alpha_3) \end{bmatrix}, \tag{5}$$

where $\ddot{\mathbf{x}}^p = \ddot{\mathbf{x}}^{p1} = \ddot{\mathbf{x}}^{p2} = \ddot{\mathbf{x}}^{p3}$. The functions of α_i on the right-hand side of equation (5) represent the acceleration corrected for instrument characteristics. The exact accelerations for the frame $\mathbf{x}^p$ may then be obtained by the inversion of equation (5).

In actual instruments, the pendulums may be misaligned so that their sensitive axes are no longer mutually perpendicular (Trifunac and Hudson, 1970). As a result, equations (2), (3), and (4) yield only three equations for the six components of acceleration. Of these six components, however, only three are independent. Therefore, coordinate transformations are required to relate the frames: $\mathbf{x}^{pi}$, $i = 1, 2, 3$. These transformations are described in the following section.

The Effect of Misalignment

For a typical accelerograph, the angles of misalignment of its transducers in the longitudinal, transverse, and vertical directions may be defined as in Figure 3. Three angles, θ, φ, and ψ, are required to determine the position of each pendulum with respect to a given reference frame $\mathbf{x} = (x_1, x_2, x_3)$. This reference frame may be chosen arbitrarily, although, for most practical purposes it is taken to coincide with the instrument casing (Figure 1).

As an example, we consider the misalignment of the x_1-pendulum in Figure 3. The motion recorded by this pendulum can be referred to as the motion in the frame $\mathbf{x}^{p1}$ in which the x_1-pendulum is perfectly aligned (Figure 4a). The coordinate systems $\mathbf{x}$ and $\mathbf{x}^{p1}$ differ by the angles φ_1, θ_1, and ψ_1 (Figure 3) and can be related through three consecutive rotational transformations which are

(1) Rotation about the x_1-axis: $\mathbf{T}_1(\eta)$

$$\begin{bmatrix} x_1' \\ x_2' \\ x_3' \end{bmatrix} = \begin{bmatrix} 1 & 0 & 0 \\ 0 & \cos\eta & \sin\eta \\ 0 & -\sin\eta & \cos\eta \end{bmatrix} \begin{bmatrix} x_1 \\ x_2 \\ x_3 \end{bmatrix} = \mathbf{T}_1(\eta)\mathbf{x}. \tag{6}$$

(2) Rotation about the x_2-axis: $\mathbf{T}_2(\eta)$

$$\begin{bmatrix} x_1' \\ x_2' \\ x_3' \end{bmatrix} = \begin{bmatrix} \cos\eta & 0 & -\sin\eta \\ 0 & 1 & 0 \\ \sin\eta & 0 & \cos\eta \end{bmatrix} \begin{bmatrix} x_1 \\ x_2 \\ x_3 \end{bmatrix} = \mathbf{T}_2(\eta)\mathbf{x}. \tag{7}$$

(3) Rotation about the x_3-axis: $\mathbf{T}_3(\eta)$

$$\begin{bmatrix} x_1' \\ x_2' \\ x_3' \end{bmatrix} = \begin{bmatrix} \cos\eta & \sin\eta & 0 \\ -\sin\eta & \cos\eta & 0 \\ 0 & 0 & 1 \end{bmatrix} \begin{bmatrix} x_1 \\ x_2 \\ x_3 \end{bmatrix} = \mathbf{T}_3(\eta)\mathbf{x}. \tag{8}$$

With the transformations defined as above, the motion with respect to the reference frame (x_1, x_2, x_3) may be transformed to the x_1-pendulum frame $\mathbf{x}^{p1}$. The following steps may be chosen:

(a) Rotate the $\mathbf{x}$ frame about the x_3-axis through an angle of φ_1 to obtain the first intermediate system x' as

$$\mathbf{x}' = \mathbf{T}_3(\varphi_1)\mathbf{x}. \tag{9}$$

This transformation aligns the x_1-pendulum so that the projection of its arm onto the x_1x_2-plane now matches the projection of the $x_2{}^{p1}$-axis as shown in Figure 3.

(b) Rotate the $\mathbf{x}_1'$ frame about the x_1'-axis through an angle θ_1 to obtain the second intermediate system $\mathbf{x}''$ as

$$\mathbf{x}'' = \mathbf{T}_1(\theta_1)\mathbf{x}'. \tag{10}$$

After this transformation, the x_2'' axis already coincides with the $x_2{}^{p1}$-axis.

(c) Finally, rotate the $\mathbf{x}''$ frame about the x_2''-axis through an angle ψ_1, Figure 3, so that the final coordinate system matches the $\mathbf{x}^{p1}$ frame, i.e.

$$\mathbf{x}^{p1} = \mathbf{T}_2(\psi_1)\mathbf{x}'' = \mathbf{T}_2(\psi_1)\mathbf{T}_1(\theta_1)\mathbf{T}_3(\varphi_1)\mathbf{x}. \tag{11}$$

Through these three rotations, we have defined the transformation $\mathbf{X}^{p1}$ as

$$\mathbf{X}^{p1} = \mathbf{T}_2(\psi_1)\mathbf{T}_1(\theta_1)\mathbf{T}_3(\varphi_1) \tag{12}$$

so that

$$\mathbf{x}^{p1} = \mathbf{X}^{p1}\mathbf{x}.$$

The elements of the transformation $\mathbf{X}^{p1}$ may be obtained by matrix multiplication as

$$\begin{bmatrix} X_{11}^{p1} & X_{12}^{p1} & X_{13}^{p1} \\ X_{21}^{p1} & X_{22}^{p1} & X_{23}^{p1} \\ X_{31}^{p1} & X_{32}^{p1} & X_{33}^{p1} \end{bmatrix} = \begin{bmatrix} \cos\psi_1\cos\varphi_1 - \sin\psi_1\sin\theta_1\sin\varphi_1 & \cos\psi_1\sin\varphi_1 + \sin\psi_1\sin\theta_1\cos\varphi_1 & -\sin\psi_1\cos\theta_1 \\ -\cos\theta_1\sin\varphi_1 & \cos\theta_1\cos\varphi_1 & \sin\theta_1 \\ \sin\psi_1\cos\varphi_1 + \cos\psi_1\sin\theta_1\sin\varphi_1 & \sin\psi_1\sin\varphi_1 - \cos\psi_1\sin\theta_1\cos\varphi_1 & \cos\psi_1\cos\theta_1 \end{bmatrix}. \tag{13}$$

To obtain a similar relation between $\mathbf{x}^{p2}$, the x_2-pendulum frame, and $\mathbf{x}$, we must go through a similar sequence of transformations because the set of misalignment angles φ_2, θ_2, and ψ_2 are in general different from those of the x_1-pendulum.

The sequential rotations may be done in the following order:

(a) Rotate about x_3-axis by φ_2 to obtain $\mathbf{x}'$.

(b) Rotate about x_2'-axis by θ_2 to obtain $\mathbf{x}''$.

(c) Rotate about x_1''-axis by ψ_2 to obtain $\mathbf{x}^{p2}$.

Therefore

$$\mathbf{x}^{p2} = \mathbf{X}^{p2}\mathbf{x} \tag{14}$$

where

$$\mathbf{X}^{p2} = \mathbf{T}_1(\psi_2)\mathbf{T}_2(\theta_2)\mathbf{T}_3(\varphi_2).$$

The elements of $\mathbf{X}^{p2}$ are then

$$\begin{bmatrix} X_{11}^{p2} & X_{12}^{p2} & X_{13}^{p2} \\ X_{21}^{p2} & X_{22}^{p2} & X_{23}^{p2} \\ X_{31}^{p2} & X_{32}^{p2} & X_{33}^{p2} \end{bmatrix} = \begin{bmatrix} \cos\theta_2\cos\varphi_2 & \\ -\cos\psi_2\sin\varphi_2 + \sin\psi_2\sin\theta_2\cos\varphi_2 & \\ \sin\psi_2\sin\varphi_2 + \cos\psi_2\sin\theta_2\cos\varphi_2 & \end{bmatrix}$$

$$\begin{bmatrix} \cos\theta_2\sin\varphi_2 & -\sin\theta_2 \\ \cos\psi_2\cos\varphi_2 + \sin\psi_2\sin\theta_2\sin\varphi_2 & \sin\psi_2\cos\theta_2 \\ -\sin\psi_2\cos\varphi_2 + \cos\psi_2\sin\theta_2\sin\varphi_2 & \cos\psi_2\cos\theta_2 \end{bmatrix}. \tag{15}$$

Similarly, the transformations for the x_3-pendulum can be

(a) Rotate about x_1-axis by φ_3 to obtain $\mathbf{x}'$.

(b) Rotate about x_3'-axis by θ_3 to obtain $\mathbf{x}''$.

(c) Rotate about x_2''-axis by ψ_3 to obtain $\mathbf{x}^{p3}$.

Hence,

$$\mathbf{x}^{p3} = \mathbf{X}^{p3}\mathbf{x}, \tag{16}$$

where

$$\mathbf{X}^{p3} = \mathbf{T}_2(\psi_3)\mathbf{T}_3(\theta_3)\mathbf{T}_1(\varphi_3), \quad \text{or}$$

$$\begin{bmatrix} X_{11}^{p3} & X_{12}^{p3} & X_{13}^{p3} \\ X_{21}^{p3} & X_{22}^{p3} & X_{23}^{p3} \\ X_{31}^{p3} & X_{32}^{p3} & X_{33}^{p3} \end{bmatrix} = \begin{bmatrix} \cos\psi_3\cos\theta_3 & \cos\psi_3\sin\theta_3\cos\varphi_3 + \sin\psi_3\sin\varphi_3 \\ -\sin\theta_3 & \cos\theta_3\cos\varphi_3 \\ \sin\psi_3\cos\theta_3 & \sin\psi_3\sin\theta_3\cos\varphi_3 - \cos\psi_3\sin\varphi_3 \end{bmatrix}$$

$$\begin{bmatrix} \cos\psi_3\sin\theta_3\sin\varphi_3 - \sin\psi_3\cos\varphi_3 \\ \cos\theta_3\sin\varphi_3 \\ \sin\psi_3\sin\theta_3\sin\varphi_3 + \cos\psi_3\cos\varphi_3 \end{bmatrix}. \tag{17}$$

Since the matrices $\mathbf{X}^{p1}$, $\mathbf{X}^{p2}$, and $\mathbf{X}^{p3}$, are independent of time, the accelerations measured in the frames $\mathbf{x}^{p1}$, $\mathbf{x}^{p2}$, and $\mathbf{x}^{p3}$ may be related to the three components of the reference frame accelerations, $\ddot{\mathbf{x}}$, by

$$\ddot{\mathbf{x}}^{pi} = \mathbf{X}^{pi}\ddot{\mathbf{x}}, \qquad i = 1, 2, 3, \tag{18}$$

i.e., accelerations $\ddot{\mathbf{x}}^{pi}$ are just the linear combination of $\ddot{\mathbf{x}}$.

The reader should note that the x_3-pendulum as illustrated in Figure 3 is placed along the x_2-axis. In different instruments, however, this pendulum may be oriented in any direction within the x_1x_2-plane as long as its sensitivity axis points in the x_3-direction. In those cases, the matrix $\mathbf{X}^{p3}$ needs to be redefined according to the coordi-

nate system used. The arrangement of pendulums shown in Figure 1 corresponds to that of the Kinemetrics SMA-1 accelerograph which is commercially produced in the United States.

Assuming that the angles φ_i, θ_i, and ψ_i for a particular instrument are determined, the exact accelerations $\ddot{\mathbf{x}}$ can now be related to the recorded accelerations α_i (obtained from the recorded traces) by combining equations (2), (3), and (4) with equations (18). After some manipulation, the matrix equation for $\ddot{\mathbf{x}}$ becomes

$$\begin{bmatrix} X_{11}^{p1}\cos\alpha_1 + X_{21}^{p1}\sin\alpha_1 & X_{12}^{p1}\cos\alpha_1 + X_{22}^{p1}\sin\alpha_1 & X_{13}^{p1}\cos\alpha_1 + X_{23}^{p1}\sin\alpha_1 \\ X_{21}^{p2}\cos\alpha_2 + X_{11}^{p2}\sin\alpha_2 & X_{22}^{p2}\cos\alpha_2 + X_{12}^{p2}\sin\alpha_2 & X_{23}^{p2}\cos\alpha_2 + X_{13}^{p2}\sin\alpha_2 \\ X_{31}^{p3}\cos\alpha_3 - X_{21}^{p3}\sin\alpha_3 & X_{32}^{p3}\cos\alpha_3 - X_{22}^{p3}\sin\alpha_3 & X_{33}^{p3}\cos\alpha_3 - X_{23}^{p3}\sin\alpha_3 \end{bmatrix}$$

$$\cdot \begin{bmatrix} \ddot{x}_1 \\ \ddot{x}_2 \\ \ddot{x}_3 \end{bmatrix} = \begin{bmatrix} r_1(\ddot{\alpha}_1 + 2\omega_{n1}\zeta_1\dot{\alpha}_1 + \omega_{n1}^2\alpha_1) \\ r_2(\ddot{\alpha}_2 + 2\omega_{n2}\zeta_2\dot{\alpha}_2 + \omega_{n2}^2\alpha_2) \\ r_3(\ddot{\alpha}_3 + 2\omega_{n3}\zeta_3\dot{\alpha}_3 + \omega_{n3}^2\alpha_3) \end{bmatrix} \tag{19}$$

or

$$\mathbf{B}\ddot{\mathbf{x}} = \ddot{\mathbf{b}}. \tag{20}$$

The coefficients of matrix $\mathbf{B}$ depend on the known misalignment angles φ_i, θ_i, and ψ_i and the deflection angles of the pendulums, α_i, while the vector $\ddot{\mathbf{b}}$ depends on the transducer constants r_i, ζ_i, ω_{ni}, as well as on the angles α_i, $\dot{\alpha}_i$, and $\ddot{\alpha}_i$. The transducer constants and misalignment angles can be obtained by calibration and static tilt tests which will be outlined in a later discussion. [Note: if the misalignment angles are all zero, equation (19) reduces to equation (5).] The deflection angles, α_i, may be obtained from the recorded accelerograms. The relation of α_i with the trace record is usually different for each instrumental design. For the SMA-1 accelerograph, for example

$$\tan 4\alpha_i = \frac{\text{trace amplitude in mm}}{125 \text{ mm}}. \tag{21}$$

The factor of $4\alpha_i$ (Figure 2) as mentioned earlier, comes from multiple reflections through a set of two mirrors, one of which is mounted on the moving pendulum, while the other is rigidly fixed to the instrument base. The distance between the moving mirror and the film for this particular instrument is 125 mm. For an acceleration of 1 g, the deflection α is approximately 2° or 0.035 rad, hence, $\tan 4\alpha$ may be approximated by 4α. After the values of α_i are digitized from the recorded traces, $\dot{\alpha}_i$ and $\ddot{\alpha}_i$ may be obtained by numerical differentiation of α_i with respect to time. These differentiating operations are feasible if the data processing procedure of Trifunac (1972) is applied.

Examples of Cross-Axis Sensitivity and Misalignment Effects

To illustrate the misalignment and cross-axis sensitivity effects we have chosen to analyze first the three components of acceleration (N 76°W, S 14°W, and DOWN) recorded at the Pacoima Dam during the 1971 San Fernando earthquake. These accelerograms were chosen partly because of their large amplitudes and partly because they probably characterize what may be, so far, the "worst case" conditions for misalignment and cross-axis sensitivity effects. The following two cases have been

studied: (a) the effects caused by cross-axis sensitivity only, i.e., assuming that the transducers are perfectly aligned and (b) the effects caused by misalignment, the angles φ_i, θ_i, and ψ_i, $i = 1, 2, 3$, being arbitrarily chosen within a reasonable range (Trifunac and Hudson, 1970), for demonstration purposes only (Table 1).

TABLE 1

ANGLES ARBITRARILY SELECTED TO CHARACTERIZE MISALIGNMENT

Angles	$i = 1$	$i = 2$	$i = 3$
φ_i	−2.50°	−4.00°	−1.50°
θ_i	−3.25°	2.50°	2.00°
ψ_i	3.00°	1.00°	−3.50°

Figure 5 shows the first 20 sec of strong-motion accelerations recorded at the Pacoima Dam site during the February 9, 1971 California earthquake. The amplitudes of these accelerations are among the largest recorded so far. The accelerations in Figure 5 were recorded by an accelerograph of the type shown in Figure 1, and we assume the instrument had natural frequencies of the transducers equal to 26 Hz

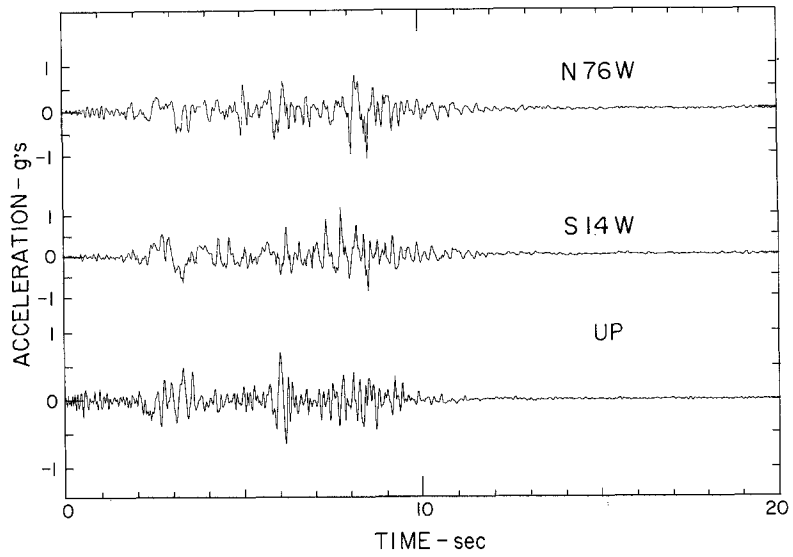

FIG. 5. Pacoima Dam accelerogram, recorded during the February 9, 1971 San Fernando earthquake in California.

and damping $\zeta = 0.65$ of critical. Furthermore, if it is assumed that the transducers in this hypothetical instrument are perfectly aligned (i.e., φ_i, θ_i, and ψ_i, $i = 1, 2, 3$, are all zero), then equations (5) present the relations between $\ddot{\mathbf{x}}$ and the recorded deflection $\boldsymbol{\alpha}$ where only the cross-axis effects are present. These equations can be used to reconstruct $\ddot{\mathbf{x}}$, the exact accelerations in the directions x_1, x_2, and x_3. Figure 6 presents the difference between recorded and corrected accelerations under those conditions for the Pacoima Dam site and shows that the overall amplitudes of the deflections do not exceed a level of about 0.03 g. The differences are clearly largest when one or more components of recorded motions display larger amplitudes, but typically are not more than several per cent of the recorded peak amplitudes.

Figure 7 shows the results of the second hypothetical experiment where the transducers in the instrument shown in Figure 1 were assumed to be misaligned by the amount shown in Table 1. With the help of equations (19) it was again possible to calculate $\ddot{\mathbf{x}}$ from the recorded $\boldsymbol{\alpha}$ and find the differences between the recorded and exact computed accelerations. These differences, shown in Figure 7, do not exceed 0.06 g.

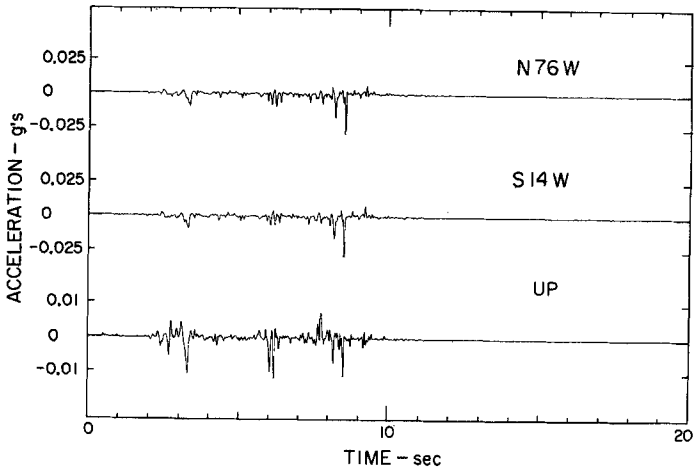

FIG. 6. Differences between the recorded and computed exact accelerations for the Pacoima Dam accelerograph which would result from cross-axis sensitivity effects alone.

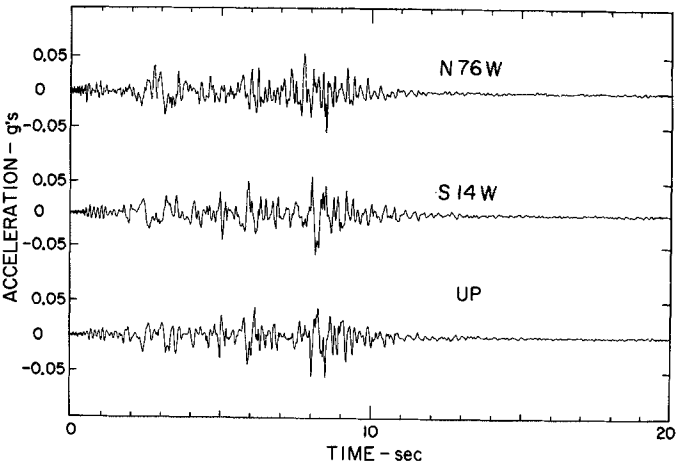

FIG. 7. Differences between the recorded and computed exact accelerations for the Pacoima Dam accelerograph which would result from misalignment of transducer pendulums (Table 1).

Results presented in Figures 6 and 7, although dependent on the particular time histories recorded at the Pacoima Dam site, may nevertheless be considered to illustrate almost the largest cross-axis sensitivity and misalignment effects that are likely to be experienced by the accelerographs of the type shown in Figure 1. Since both misalignment and cross-axis sensitivity effects are accentuated by simultaneous large accelerations in the direction of coordinate pairs (x_1^{p1}, x_2^{p1}), (x_1^{p2}, x_2^{p2}), and (x_2^{p3}, x_3^{p3}) (Figure 4), it is clear that with a decrease of the overall levels of shaking, the significance of these effects would also diminish.

To illustrate this we studied the accelerogram recorded in the basement of the Alexander Building in San Francisco during the March 22, 1957 earthquake in San Francisco. The recorded amplitudes of accelerations for this event did not exceed about 0.05 g (Figure 8). As shown in Figures 9 and 10, the effects of cross-axis sensitivity alone and of misalignment did not contribute more than 0.5×10^{-4} g and 0.3×10^{-3} g, respectively.

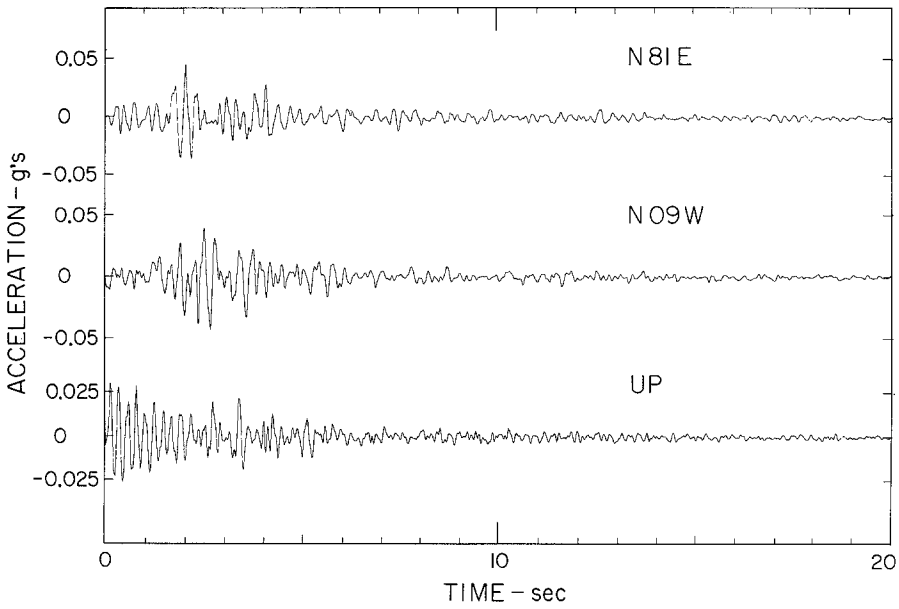

FIG. 8. Acceleration recorded in the basement of the Alexander Building, San Francisco, on March 22, 1957.

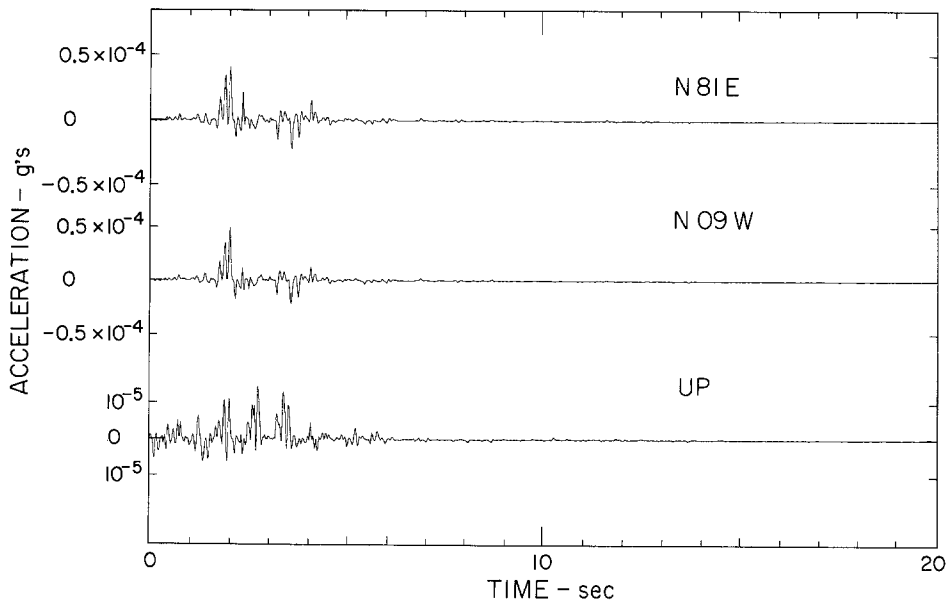

FIG. 9. Differences between the recorded and computed exact accelerations in the basement of the Alexander Building which would result from cross-axis sensitivity effects alone.

These two examples therefore suggest that the cross-axis sensitivity effects contribute something on the order of 0.1 to about 3 per cent for recorded accelerations ranging from about 0.05 g to about 1 g. This is in agreement with the work of Rogers (1975) who found these effects to be about 5 per cent of 1-g accelerations. The effects

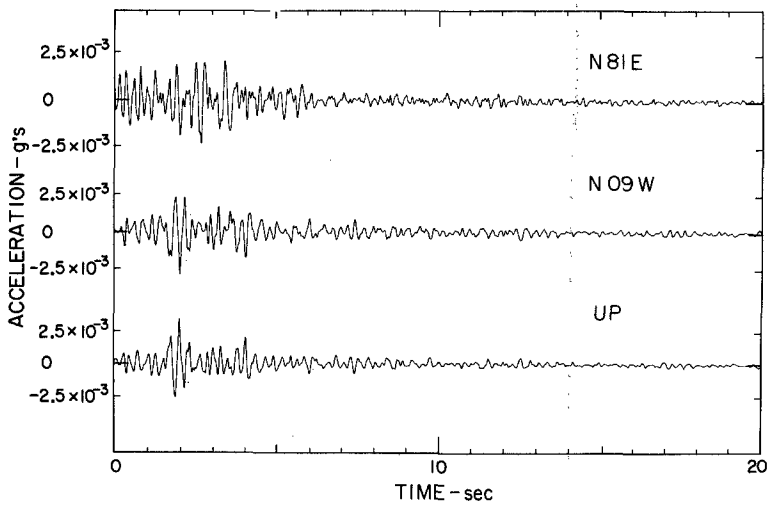

FIG. 10. Differences between the recorded and computed exact accelerations in the basement of the Alexander Building which would result from misalignment of the transducer pendulums (Table 1).

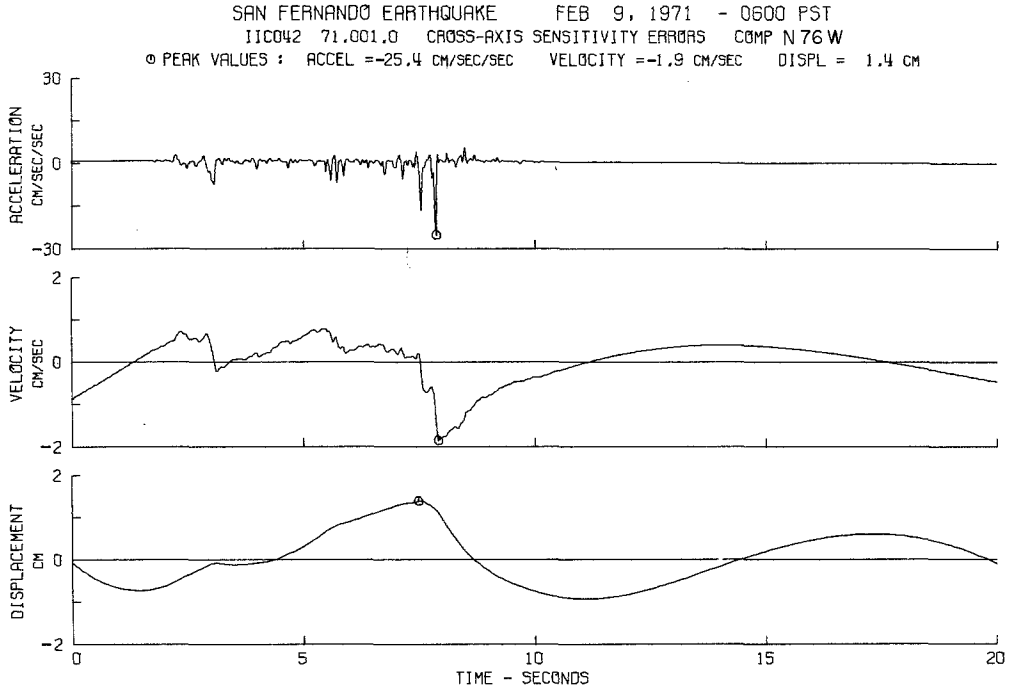

FIG. 11. Acceleration, velocity, and displacement which would result from cross-axis sensitivity effects on the recorded N76°W components of acceleration at Pacoima Dam (Figure 6). Acceleration, velocity, and displacement in the figure have been processed with the band-pass filtering methods used in the routine processing of all strong-motion accelerograms (Trifunac and Lee, 1973).

of misalignment, however, which strongly depend on actual misalignment angles ϕ_i, θ_i, and ψ_i, $i = 1, 2, 3$, probably contribute from 0.5 to about 5 per cent and more for the same range of recorded accelerations. More precise characterization of these percentages would require detailed studies of the distributions of φ_i, θ_i, and ψ_i, $i = 1, 2, 3$, for typical accelerographs and would require numerous calculations using equations (19) so as not to neglect the dependence of these effects on the particular time histories involved. Such calculations, however, do not seem worthwhile now, because the theory presented in this paper can be used without much difficulty to correct for both of these effects and thus eliminate them completely from the recorded motions.

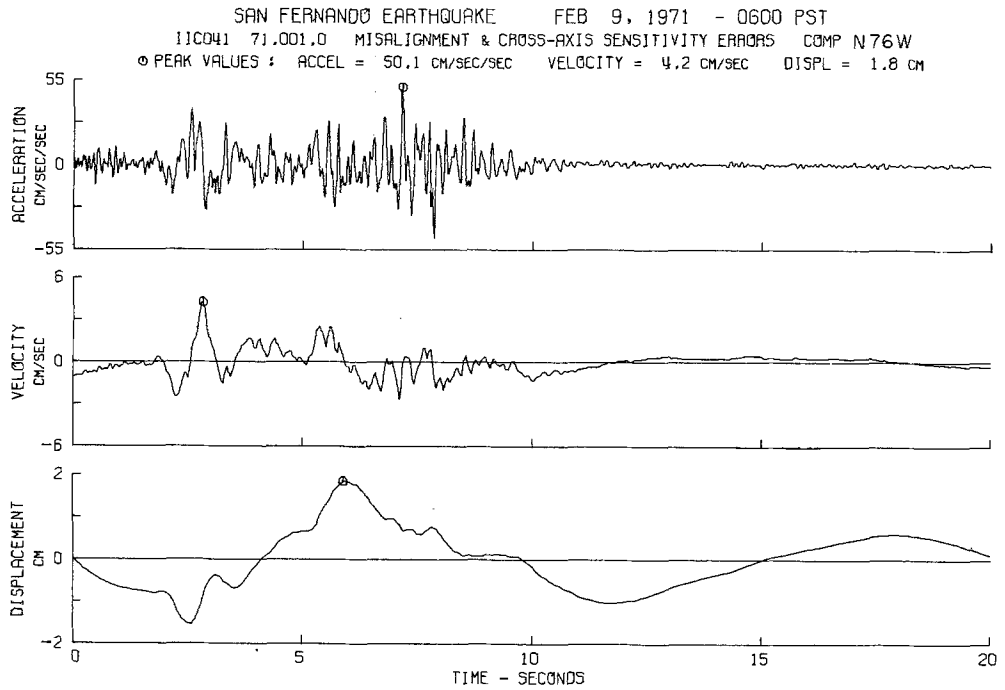

FIG. 12. Acceleration, velocity, and displacement which would result from misalignment effects on the recorded N76°W component of acceleration at Pacoima Dam (Figure 6). Acceleration, velocity, and displacement in the figure have been processed with the band-pass filtering methods used in the routine processing of all strong-motion accelerograms (Trifunac and Lee, 1973).

To show the effects of cross-axis sensitivity and misalignment of transducers on computed velocity and displacement curves and on response spectrum amplitudes, one component each from Figures 6, 7 and 10 has been selected for presentation. Further analysis of accelerograms in Figure 9 was omitted because the amplitudes which do not exceed about 0.5×10^{-4} g are smaller than the average digitization noise (Trifunac *et al.*, 1973), Figures 11, 12, 13, and 14 show the integrated velocity, displacement, and pseudo-velocity response spectra for cross-axis sensitivity alone and for cross-axis sensitivity and misalignment effects combined for the N76°W component of the Pacoima Dam accelerogram. Figures 15 and 16 present the corresponding information for the combined effects of cross-axis sensitivity and misalignment for the N81°E component of the accelerogram recorded in the basement of the Alexander Building in San Francisco. Throughout these computations the same arbitrarily se-

lected nine angles (Table 1) were assumed to characterize the misalignment angles. This particular choice of misalignment angles is believed to portray worse than average misalignment angles (Trifunac and Hudson, 1970), but the assertion of this possible fact will have to await more detailed analysis of the distribution of these angles in the installed accelerographs. Such analysis would require complete tilt testing of all existing instruments.

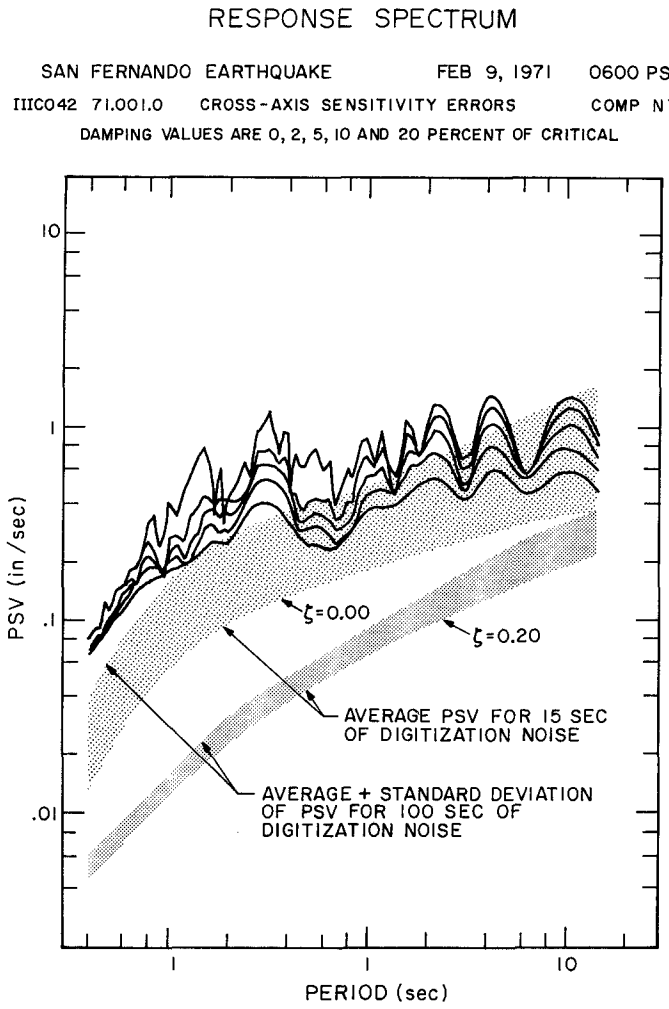

FIG. 13. N76°W PSV spectra that would result from the differences in acceleration recorded at Pacoima Dam (Figure 11) and caused by cross-axis sensitivity effects alone, compared with the range of amplitudes of PSV spectra resulting from the overall digitization noise.

Figures 11 through 16 show that the misalignment and cross-axis sensitivity effects appear to be negligible for small levels of shaking portrayed here by the accelerogram recorded in the Alexander Building. These effects, however, become noticeable and significantly larger than the digitization noise for the level of shaking recorded by the Pacoima Dam accelerograph. Figure 13 shows, for example, that the cross-axis sensitivity effects alone become comparable to and for some frequencies larger than the highest amplitudes of digitization noise. Figure 14 shows that the effects of misalign-

ment for this particular set of φ_i, θ_i, and ψ_i, $i = 1, 2, 3$ (Table 1), can lead to spectral amplitudes which are, in the higher frequency range, an order of magnitude higher than the highest amplitudes resulting from digitization noise.

The foregoing examples only suggest the overall trend and possible range of the effects that may be caused by the cross-axis sensitivity and/or misalignment of acceleration transducers of the single degree-of-freedom pendulous type. Those ex-

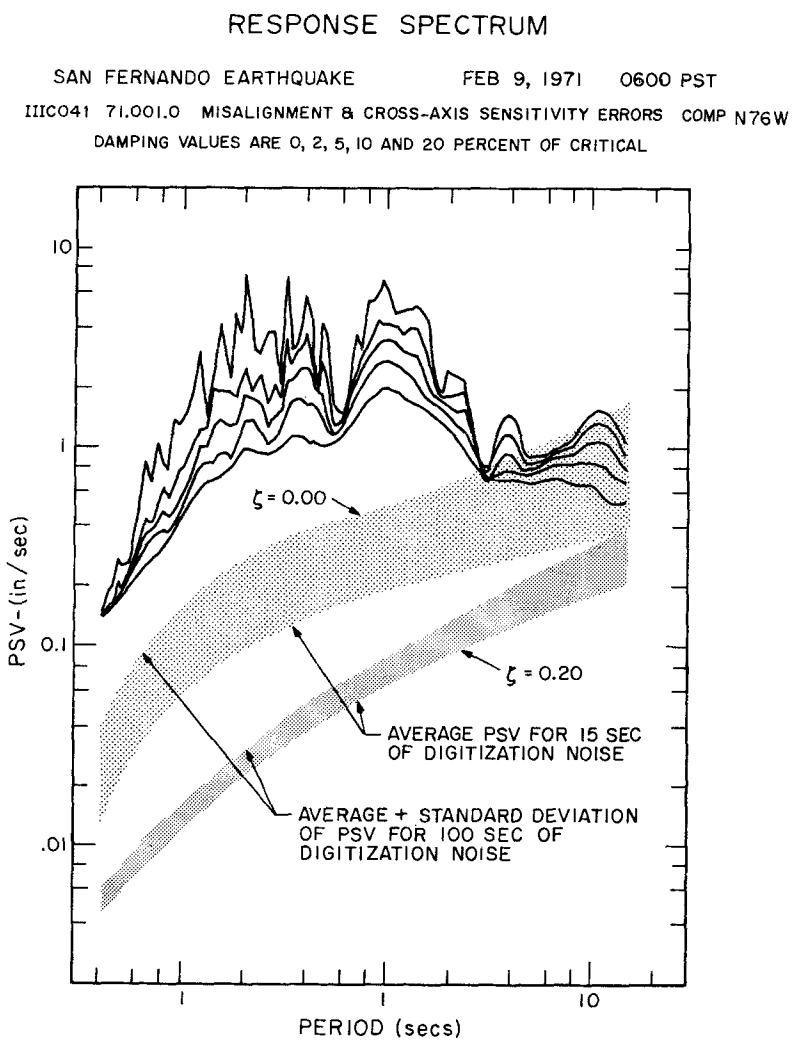

FIG. 14. N76°W PSV spectra that would result from the differences in acceleration recorded at Pacoima Dam (Figure 12) and caused by misalignment effects alone, compared with the range of amplitudes of PSV spectra resulting from the overall digitization noise.

amples cannot be interpreted to mean, for example, that whenever peak accelerations exceed 1 g the effects of misalignment will be an order of magnitude larger than those resulting from the digitization noise. Both cross-axis sensitivity effects and the misalignment effects depend on the details of excitation function, on the sensitivity of transducers, and on actual misalignment angles. A combination of all these factors will determine the overall amplitudes and spectral characteristics of these effects in each particular case.

The Approximate Characterization of Cross-Axis Sensitivity and Misalignment

Since the misalignment and deflection angles of the pendulums are typically small, the matrix **B** may be simplified by using the small angle approximation, i.e., $\sin \eta \cong \eta$ and $\cos \eta \cong 1$. Keeping only the zeroth and the first-order terms, equations (19) simplify to

$$\begin{bmatrix} 1 & \varphi_1 + \alpha_1 & -\psi_1 \\ -\varphi_2 + \alpha_2 & 1 & \psi_2 \\ \psi_3 & -\varphi_3 - \alpha_3 & 1 \end{bmatrix} \begin{bmatrix} \ddot{x}_1 \\ \ddot{x}_2 \\ \ddot{x}_3 \end{bmatrix} = \begin{bmatrix} \ddot{b}_1 \\ \ddot{b}_2 \\ \ddot{b}_3 \end{bmatrix}. \tag{22}$$

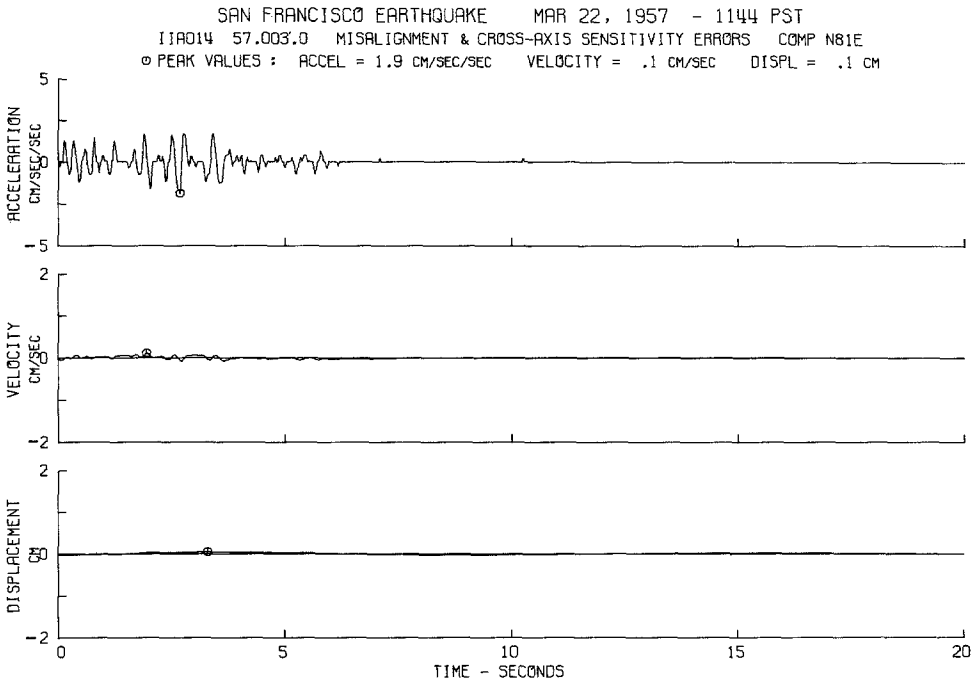

FIG. 15. Acceleration, velocity, and displacement which would result from misalignment effects on the recorded N81°E component of acceleration in the basement of the Alexander Building (Figure 10). Acceleration, velocity, and displacement in the figure have been processed with the band-pass filtering methods used in the routine processing of all strong-motion accelerograms (Trifunac and Lee, 1975).

The first-order solution for $\ddot{\mathbf{x}}$ may be obtained by Cramer's rule as

$$\begin{aligned} \ddot{x}_1 &\cong \ddot{b}_1 - (\varphi_1 + \alpha_1)\ddot{b}_2 + \psi_1 \ddot{b}_3 , \\ \ddot{x}_2 &\cong \ddot{b}_2 + (\varphi_2 - \alpha_2)\ddot{b}_1 - \psi_2 \ddot{b}_3 , \\ \ddot{x}_3 &\cong \ddot{b}_3 + (\varphi_3 + \alpha_3)\ddot{b}_2 - \psi_3 \ddot{b}_1 , \end{aligned} \tag{23}$$

where φ_i, ψ_i, and α_i are measured in radians.

Equation (23) shows clearly the significance of different angles. ψ_i contributes to the acceleration from the direction in which the transducer springs are stiffest. The angles, φ_i, may be viewed as a permanent contribution to the deflections α_i. It can

also be noticed that the effects caused by θ_i are of second order only and do not appear in equation (23). Thus, for most cases when the misalignment angles are small, the effects of θ_i can be ignored. The percentage of orthogonal acceleration, $\ddot{b}_j$, $j \neq i$, added to $\ddot{x}_i$ is approximately $\pi/180°$ or 1.75 per cent for each degree of ψ and φ.

As an "order of magnitude" check for case II: let $\varphi \approx 2.5°$ and $\psi \simeq 3°$ (Table 1). Then the acceleration contributed by the components other than principal sensitivity may be about 4 to 5% g (40 to 50 cm/sec^2) for a 1 g peak acceleration. From Figure

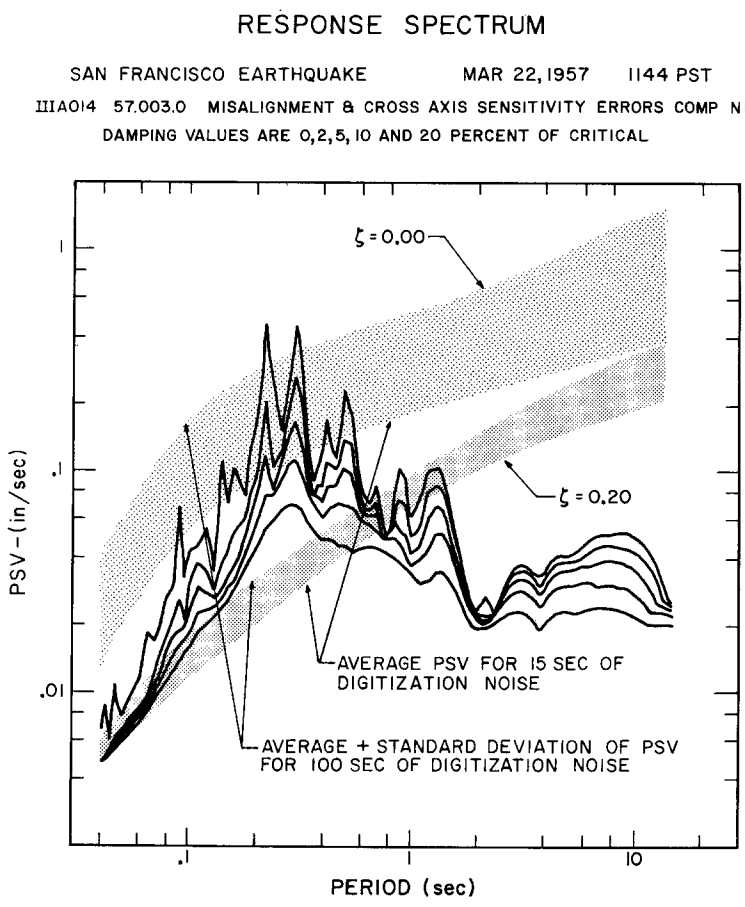

FIG. 16. N81E PSV spectra that would result from the differences in acceleration recorded in the basement of the Alexander Building (Figure 15) and caused by misalignment effects, compared with the range of amplitudes of PSV spectra resulting from the overall digitization noise.

10 it is seen that the computed differences are approximately 50 to 60 cm/sec^2; hence, the above estimate of the amplitudes of this effect may be acceptable. The cross-axis sensitivity contributions to the deflection angles, α_i, however, are of a different nature because α_i are variables which depend primarily on the acceleration $\ddot{b}_i$, to a lesser degree on $\ddot{b}_j$, $j \neq i$, and can be influenced by the constraints which are imposed during the practical considerations of the transducer design (Rogers, 1975).

As an approximation, we can write

$$\alpha_i \approx S_i \ddot{b}_i \tag{24}$$

where S_i is the "sensitivity" of the x_i-pendulum (in units of radian per unit acceleration). Assuming for a moment that ψ_i, φ_i, and θ_i are zero and applying the relations (24), equations (23) reduce to

$$\ddot{x}_1 \cong \ddot{b}_1 - S_1\ddot{b}_1\ddot{b}_2$$

$$\ddot{x}_2 \cong \ddot{b}_2 - S_2\ddot{b}_1\ddot{b}_2$$

$$\ddot{x}_3 \cong \ddot{b}_3 + S_3\ddot{b}_2\ddot{b}_3 \,. \tag{25}$$

This new form of (23) indicates that the differences between $\ddot{\mathbf{x}}$ and $\ddot{\mathbf{b}}$ are large only when the corresponding cross-axis accelerations are large simultaneously. Hence, if one or both accelerations are small, the differences are also small as indicated by the beginning and ending parts of $\ddot{\mathbf{x}} - \ddot{\mathbf{b}}$ in Figures 6 and 9. Equations (25) also explain why the horizontal traces plotted in Figures 6 and 9 are so similar.

To check the amplitudes of the differences shown in Figure 6, we assume that $\ddot{b}_1$ and $\ddot{b}_2$ reach a 1-g acceleration at the same time. With $S \approx 0.035$ rad/g for the assumed SMA-1 accelerograph, the maximum difference $\ddot{x}_1 - \ddot{b}_1$ should be approximately $S\ddot{b}_1\ddot{b}_2 \approx (0.035 \text{ rad}/g)(1\ g)^2 \approx 3.5\,\%\ g$ or 35 cm/sec^2. The differences indicated in Figure 6 are approximately equal to 30 cm/sec^2, indicating that this approximate calculation of cross-axis effects does agree with the exact differences based on equations (19).

Calibration and Static Tilt Tests

To determine the transducer constants and misalignment angles, standard calibration tests can be performed (Trifunac and Hudson, 1970). The natural frequency and damping of each transducer can both be measured in addition to the results of factory tests which are provided by the manufacturers. The actual misalignment angles of the transducers which reflect the imperfect positioning of individual transducers are currently not provided by the manufacturers and have to be determined by additional laboratory testing. In factory testing of SMA-1 accelerographs, for example, only simple tests are made to ensure that the misalignment effect does not exceed $\pm 0.04\ g/g$ during static tilt tests.

In this section, we present two methods for the calculation of misalignment angles. The first method leads to an algorithm which can accurately determine the angles φ, θ, and ψ, but has the disadvantage that it requires very accurate data from the tilt tests. For this reason, a simple approximate (second) method has also been presented. This latter method gives good results which appear to be off less than 5 per cent from the first and more accurate method for determining φ and ψ, but has the disadvantage that the angle θ cannot be determined. The reason for this deficiency may readily be explained by the first-order equations (23), where the angle θ is absent. This shows that the misalignment effects caused by θ contribute to the recorded acceleration only in a second-order manner.

Method I. The static tilt test, where the acceleration of gravity is utilized as the source of excitation, has been used extensively as a convenient means for determining the transducer sensitivity as well as misalignments (Skinner and Stephenson, 1973; Trifunac and Hudson, 1970). During a tilt test, the instrument is rotated about a selected axis and away from its normal operating orientation so that all transducer sensitivity axes receive a fraction of 1 g of static acceleration.

A series of tilt tests that may be performed is illustrated in Figure 17 as follows

$$\begin{aligned}
&\text{I. } x_3\text{-axis up:} && \ddot{x}_1 = 0, \quad \ddot{x}_2 = 0, \quad \ddot{x}_3 = 1\,g \\
&\text{II. } x_2\text{-axis down:} && \ddot{x}_1 = 0, \quad \ddot{x}_2 = -1\,g, \quad \ddot{x}_3 = 0 \\
&\text{III. } x_2\text{-axis up:} && \ddot{x}_1 = 0, \quad \ddot{x}_2 = 1\,g, \quad \ddot{x}_3 = 0 \\
&\text{RETURN TO POSITION I FOR A CHECK.} \\
&\text{IV. } x_1\text{-axis down:} && \ddot{x}_1 = -1\,g, \quad \ddot{x}_2 = 0, \quad \ddot{x}_3 = 0 \\
&\text{V. } x_1\text{-axis up:} && \ddot{x}_1 = 1\,g, \quad \ddot{x}_2 = 0, \quad \ddot{x}_3 = 0 \\
&\text{VI. } x_3\text{-axis down:} && \ddot{x}_1 = 0, \quad \ddot{x}_2 = 0, \quad \ddot{x}_3 = -1\,g \qquad (26) \\
&\text{RETURN TO POSITION I FOR A CHECK.}
\end{aligned}$$

Other combinations of tilts may be carried out to obtain the same results, but the sequence described above which consists of 90° tilts only avoids the necessity of having sophisticated tilt tables. All other tilt accelerations may be expressed as a linear combination of the above six.

The deflections of the pendulums, α_i, recorded on film or paper during these tilt tests are related to $\ddot{\mathbf{x}}$ by equations (19). The right-hand side, $\ddot{\mathbf{b}}$, for these tests is just $\{r_1\omega_{n1}^2\alpha_1, r_2\omega_{n2}^2\alpha_2, r_3\omega_{n3}^2\alpha_3\}^T$ because $\ddot{\alpha}_i$ and $\dot{\alpha}_i$ are zero for static conditions. With $\ddot{\mathbf{x}}$ and $\ddot{\mathbf{b}}$ known, the unknowns in equation (19) are the values X_{ij}^{pl}, $i, j, l = 1, 2, 3$. For each pendulum, only six of nine values for X_{ij}^{pl} contribute to the record because the pendulums are assumed to be rigid in one direction.

The deflection patterns of all three pendulums during the sequence of tilt tests (Figure 17) are shown in Figure 18a, where the solid lines, dashed lines, and dotted lines represent the responses of the x_1-, x_2-, and x_3-pendulums, respectively. The deflections ξ_{ij}^+ and ξ_{ij}^- for each tilt are defined by

$$\begin{aligned}
&\xi_{ij}^+ \equiv \text{deflection of the } x_i\text{-pendulum when } x_j\text{-axis is pointing upward (Figure 17)} \\
&\xi_{ij}^- \equiv \text{deflection of the } x_i\text{-pendulum when } x_j\text{-axis is pointing downward (Figure 17).} \qquad (27)
\end{aligned}$$

By rearranging and grouping the deflection traces for each pendulum as shown in Figure 18b, one can see that the largest deflections of the three sets are $\xi_{ij}^{\pm}$ when $i = j$, i.e., when $1\,g$ or $-1\,g$ is applied in the direction of the sensitive axis x_i. In general if the transducers are perfectly aligned, the difference $\xi_{ij}^+ - \xi_{ij}^- = 2\,g$ for $i = j$ and zero for $i \neq j$. The latter is true because the cross-axis accelerations cannot cause a deflection in a particular pendulum unless it is perturbed from its equilibrium position. Hence, under ideal conditions the four deflection amplitudes ξ_{ij}^+ and ξ_{ij}^- for $i \neq j$ of Figure 18b would collapse into one line. However, if misalignments exist, the cross-axis acceleration can easily be detected, and the deflection patterns for such cases may be quite similar to those shown in Figure 18b.

It should be noted here that the trace of the vertical transducer ξ_{33}^-, shown in Figure 18a, may go off scale if the sensitivity of this transducer is larger than ($\frac{1}{4}$ of the total record width)/g, i.e., ~1.75 cm/g for instruments using 70-mm film, and when the

recording trace is positioned centrally on paper or film. This could be avoided by positioning vertical transducer so that ξ_{33}^{+} is slightly off the center (up in Figure 18a) or by interchanging the recording positions of traces for x_1- and x_3-pendulums. When neither of these alternatives are feasible or convenient, additional tilt tests can be performed to calculate the amplitude ξ_{33}^{-}. The optimum solution of this will, of course, depend on each particular instrument and on the characteristics imposed by practical aspects of routine calibration tests.

To carry out the calculation of the angles φ_i, θ_i, and ψ_i, we must know the exact position of the base lines z_i as shown in Figure 18b. These base lines correspond to the positions of the pendulums which are not subjected to any accelerations and are difficult to determine experimentally because we cannot easily carry out the tests in the absence of gravity. However, it can be seen that z_i is located between the pairs of deflections ξ_{ij}^{+} and ξ_{ij}^{-}, because during these tests each pendulum is subjected to both

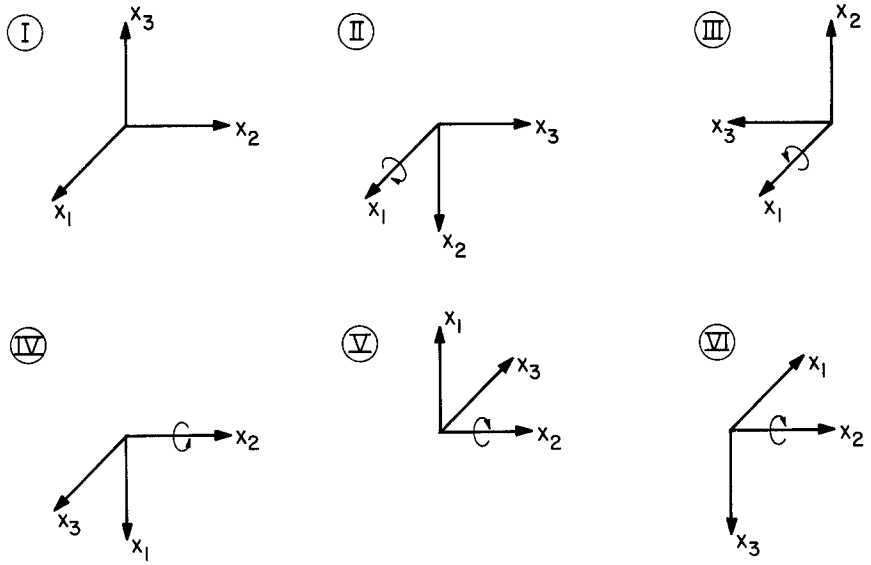

FIG. 17. Series of static tilt tests designed for the computation of misalignment angles φ_i, θ_i, and ψ_i, $i = 1, 2, 3$, relative to the x_1, x_2, x_3 coordinate system.

1 g and -1 g acceleration in the x_j-direction; the deflections of the pendulums $(\xi_{ij}^{+} - z_i)$ and $(\xi_{ij}^{-} - z_i)$ from their base-line position, z_i, then must also have opposite signs.

Using equation (21), the deflection angles α_{ij}^{+} may be calculated from the trace deflections $(\xi_{ij}^{\pm} - z_i)$ as

$$\alpha_{ij}^{\pm} = \frac{1}{4} \tan^{-1} \left[\frac{(\xi_{ij}^{\pm} - z_i) \text{ mm}}{125 \text{ mm}} \right]. \tag{28}$$

Then one can use equations (19) for the calculation of unknowns X_{ij}^{pl} as soon as the positions of z_i are established.

For example, one can consider the case of the x_1-pendulum: the substitution of the six independent accelerations, $\ddot{x}_1 = \pm 1$ g, $\ddot{x}_2 = \pm 1$ g, and $\ddot{x}_3 = \pm 1$ g corresponding to the tilt tests I through VI, into equations (19) would yield six independent equa-

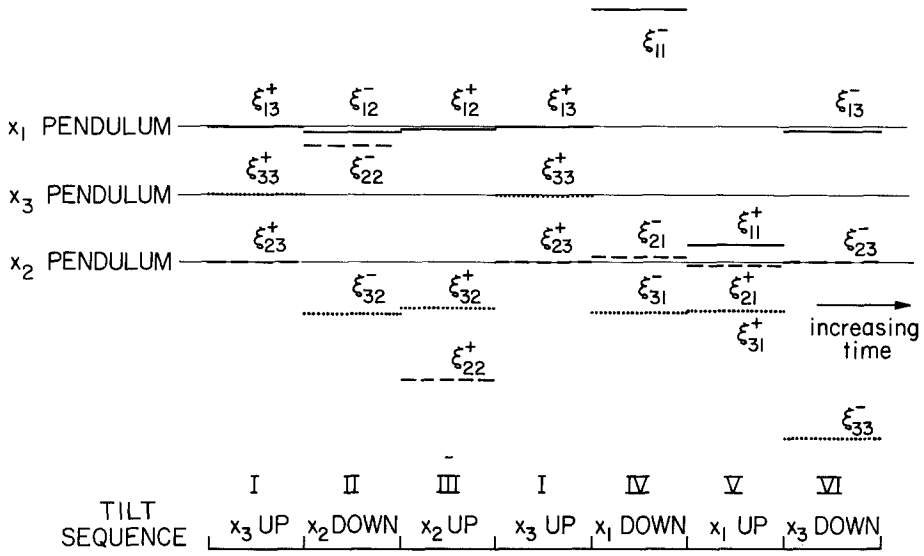

FIG. 18a. An example of recorded transducer displacements which would result from tilt tests shown in Figure 17. Continuous light lines show the position of the three traces under normal operating conditions with x_3 pointing up.

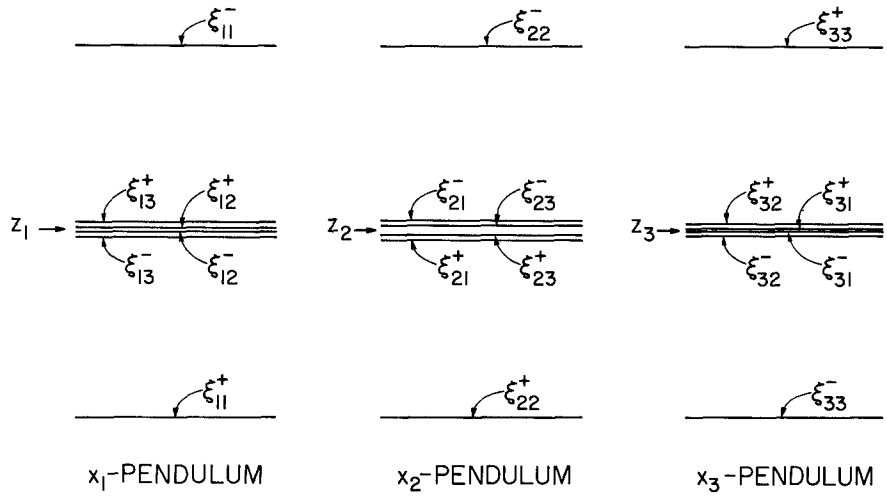

FIG. 18b. Deflections of x_1-, x_2-, and x_3-pendulum traces for six tilts shown in Figure 17. z_1, z_2, and z_3 represent the positions of these traces which would be obtained in the absence of any gravitational field.

tions for six unknowns

$$(+1\ g)[X_{1j}^{p1} \cos \alpha_{1j}^{+} + X_{2j}^{p1} \sin \alpha_{1j}^{+}] = C_1 \alpha_{1j}^{+}$$

$$(-1\ g)[X_{1j}^{p1} \cos \alpha_{1j}^{-} + X_{2j}^{p1} \sin \alpha_{1j}^{-}] = C_1 \alpha_{1j}^{-} \qquad (29)$$

$$\text{for } j = 1, 2, 3$$

where C_1 is the sensitivity constant for the x_1-pendulum measured in the units of

g/rad. After simple algebraic manipulations, the solutions of (29) are

$$X_{1j}^{p1} = -C_1\left[\frac{\alpha_{1j}^{+}\sin\alpha_{1j}^{-} + \alpha_{1j}^{-}\sin\alpha_{1j}^{+}}{\sin(\alpha_{1j}^{+} - \alpha_{1j}^{-})}\right]$$

$$X_{2j}^{p1} = C_1\left[\frac{\alpha_{1j}^{+}\cos\alpha_{1j}^{-} + \alpha_{1j}^{-}\cos\alpha_{1j}^{+}}{\sin(\alpha_{1j}^{+} - \alpha_{1j}^{-})}\right] \qquad (30)$$

$$\text{for} \quad j = 1, 2, 3,$$

where α_{1j}^{+} and α_{1j}^{-} are related to the unknown "weightless" positions z_i by equations (28).

Referring to equation (13), we can see that the six quantities X_{ij}^{p1}, $i = 1, 2$ and $j = 1, 2, 3$, depend only on three angles φ_1, θ_1, and ψ_1. Therefore, not all six quantities are needed for the calculations of the angles. The following expressions could be used

$$X_{23}^{p1} = \sin\theta_1 \Rightarrow \theta_1 = \sin^{-1}(X_{23}^{p1})$$

$$X_{13}^{p1} = -\sin\psi_1\cos\theta_1 \Rightarrow \psi_1 = -\sin^{-1}(X_{13}^{p1}/\cos\theta_1)$$

$$\left.\begin{aligned} X_{21}^{p1} &= -\cos\theta_1\sin\varphi_1 \\ X_{22}^{p1} &= \cos\theta_1\cos\varphi_1 \end{aligned}\right\} \Rightarrow \varphi_1 = -\tan^{-1}(X_{21}^{p1}/X_{22}^{p1}) \qquad (31)$$

$$\left.\begin{aligned} X_{11}^{p1} &= \cos\psi_1\cos\varphi_1 - \sin\psi_1\sin\theta_1\sin\varphi_1 \\ X_{12}^{p1}\ \mathrm{W}\ &\cos\psi_1\sin\varphi_1 + \sin\psi_1\sin\theta_1\cos\varphi_1 \end{aligned}\right\} \text{NOT USED.}$$

For any reasonable values of z_1, the angles φ_1, θ_1, and ψ_1 obtained from (31) will satisfy the equations for X_{13}^{p1} and X_{23}^{p1} exactly, and the equations for X_{21}^{p1} and X_{22}^{p1} only approximately because $\cos\theta_1$ is determined by using X_{23}^{p1}. But the equations for X_{11}^{p1} and X_{12}^{p1} must also be satisfied by these angles, and so there is only one combination of φ_1, θ_1, and ψ_1 which is valid for all six expressions X_{ij}^{p1}. Hence, the algorithm for determining the angles φ_1, θ_1, and ψ_1 may be constructed as follows:

(1) Assume a value of z_1,
(2) calculate α_{1j}^{+} and α_{1j}^{-} for $j = 1, 2, 3$;
(3) calculate X_{ij}^{p1} for $i = 1, 2$; and $j = 1, 2, 3$;
(4) determine φ_1, θ_1, and ψ_1 from X_{ij}^{p1} using equations (31);
(5) replace φ_1, θ_1, and ψ_1 into the equations for X_{ij}^{p1} and check if all six are satisfied.
(6) If yes: z_1, φ_1, θ_1, and ψ_1 are all valid answers. If not: return to step (1) and choose a better guess for z_1.

The algorithm listed above is useful provided very accurate measurements of $\xi_{ij}^{\pm}$ are available. Otherwise, the values of X_{1j}^{p1} and X_{2j}^{p1} in equation (30) may be subject to considerable errors because both the denominator, $\sin(\alpha_{1j}^{+} - \alpha_{1j}^{-})$, and the numerator represent sums and differences of quantities having nearly the same numerical value and thus may be quite sensitive to truncation errors. As an example, consider the following set of deflections

$$\xi_{11}^{+} = 0.4140 \times 10^{-1}\ \text{rad}$$

$$\xi_{11}^{-} = -0.3492 \times 10^{-1} \text{ rad}$$

$$\xi_{12}^{+} = 0.6662 \times 10^{-2} \text{ rad} \qquad \text{with } C_1 = 26\ g/\text{rad}.$$

$$\xi_{12}^{-} = 0.2906 \times 10^{-3} \text{ rad}$$

$$\xi_{13}^{+} = 0.0$$

$$\xi_{13}^{-} = 0.6695 \times 10^{-2} \text{ rad}$$

The value of z_1 which leads to a negligible error in matching the six equations for X_{ij}^{p1} is 0.33543×10^{-2}; the corresponding values for φ_1, θ_1, and ψ_1 are 4.52°, 5°, and 3°, respectively.

Method II. Because careful testing and detailed data reduction procedures are required for Method I, we present a simpler method in this section.

Returning to the six independent equations in (29), we may simplify the calculations by introducing the following assumptions

$$\alpha_{1j}^{+} \cong -\alpha_{1j}^{-} \cong \alpha_{1j} \tag{32}$$

where

$$\alpha_{1j} = \frac{\alpha_{1j}^{+} - \alpha_{1j}^{-}}{2}.$$

This assumption implies that the deflection angles caused by $1\ g$ and $-1\ g$ have approximately the same magnitude; this is generally true for all instruments with small misalignments and stiff transducer springs. Substituting the approximate relation (32) into equations (24) gives

$$\begin{aligned} X_{1j}^{p1} \cos \alpha_{1j} + X_{2j}^{p1} \sin \alpha_{1j} &= C_1 \alpha_{1j} \\ -X_{1j}^{p1} \cos \alpha_{1j} + X_{2j}^{p1} \sin \alpha_{1j} &= -C_1 \alpha_{1j} \\ j &= 1, 2, 3. \end{aligned} \tag{33}$$

The solutions for X_{1j}^{p1} are approximately

$$X_{1j}^{p1} = \frac{C_1 \alpha_{1j}}{\cos \alpha_{1j}}, \qquad j = 1, 2, 3. \tag{34}$$

$$\begin{aligned} X_{11}^{p1} &= \cos \psi_1 \cos \varphi_1 - \sin \psi_1 \sin \theta_1 \sin \varphi_1 \cong 1 \\ X_{12}^{p1} &= \cos \psi_1 \sin \varphi_1 + \sin \psi_1 \sin \theta_1 \cos \varphi_1 \cong \varphi_1 \\ X_{13}^{p1} &= -\sin \psi_1 \cos \theta_1 \cong -\psi_1 . \end{aligned} \tag{35}$$

Since X_{11}^{p1} does not contribute additional information for these angles, the approxi-

mations for φ_1 and ψ_1 may be written as follows

$$\varphi_1 \cong \frac{C_1(\alpha_{12}^+ - \alpha_{12}^-)/2}{\cos\,[(\alpha_{12}^+ - \alpha_{12}^-)/2]}$$

$$\psi_1 \cong \frac{C_1(\alpha_{13}^+ - \alpha_{13}^-)/2}{\cos\,[(\alpha_{13}^+ - \alpha_{13}^-)/2]}\,. \tag{36}$$

Similar expressions may also be derived for the x_2- and x_3-pendulums. The angles θ_i cannot be obtained by this first-order approximation.

To compare the accuracy of the expressions in (36) against the results obtained by Method I, we calculated the angles φ_1 and ψ_1 for the values of $\xi_{ij}^{\pm}$ already given. The results were φ_1 and ψ_1 for the values of $\xi_{ij}^{\pm}$ already given. The results were $\varphi_1 = 4.75°$ (5 per cent off) and $\psi_1 = 4.99°$ (less than 1 per cent off). This suggests that the approximate method may be adequate for most routine applications. Here, of course, one would select an approximate value of $\theta_1 = 0$.

Conclusions

The exact method for elimination of the effects caused by cross-axis sensitivity and misalignment of pendulous type transducers has been presented. By applying this method to the processing of the recorded accelerations, it is possible to compute the exact accelerations relative to any Cartesian coordinate system. To carry out such computations it is necessary to find the static positions of acceleration transducers relative to this coordinate system.

Illustrative examples of the quantitative significance of the cross-axis sensitivity and misalignment have been presented to characterize the order of magnitude these effects may have on typical recorded accelerograms. Although the two examples presented do not permit any generalizations, it appears that for small input accelerations (typically less than 0.05 g) contributions to recorded accelerations that result from cross-axis sensitivity and misalignment are not significantly different from the overall amplitudes of digitization and processing noise. For large accelerations (of the order of 1 g), however, these effects can be significantly above the digitization noise but do not seem to contribute much more than about 5 per cent of the recorded amplitudes. These trends are only valid for the accelerations band-pass filtered between 0.07 and 25 Hz, in the amplitude range to about 1 g for instruments whose transducers have similar characteristics to those for the SMA-1 Kinemetrics accelerograph. Other types of transducers with different amplification and geometric characteristics may lead to different overall sensitivity to cross-axis and misalignment effects.

Routinely processed strong-motion accelerograms (Trifunac and Lee, 1973) have not been corrected for cross-axis and misalignment effects because the tilt tests required for such corrections have not been performed. Whether these corrections need to be performed will have to be decided from the viewpoint of each particular analysis which employs recorded strong ground motion. Whenever such analyses utilize only the general and overall characteristics of recorded strong acceleration, it seems that additional variations caused by cross-axis sensitivity and misalignment not exceeding several percent of the recorded motions may not be important to warrant special treatment and their elimination from the available records. For detailed analyses,

however, when a high degree of accuracy is required, the effects of cross-axis sensitivity and misalignment should be eliminated from the recorded motions.

It could be required that the instruments be designed so that the misalignment of transducers is virtualy eliminated. While technically this seems to be feasible, the additional labor, the possibly rough handling of instruments before they reach their field destination, and the possible subsequent field adjustments, suggest that this may not be the optimum alternative. An instrument may be serviced many times before it records strong ground motion. During this long time interval field technicians have numerous opportunities to purposely change or accidentally alter the original adjustment of acceleration transducers. With this in mind, it seems worthwhile to explore the possibility of tilt calibrations (similar to those shown in Figure 17) of instruments following every important recording and prior to any type of interference with or adjustments of the transducers. In this way the misalignments of accelerometers would be calibrated while they are still in the configuration identical to that during which the recording took place. With the data from such calibrations and by employing the correction procedures outlined in this paper, both cross-axis sensitivity and misalignment effects would be completely removed.

In summary, it might be pointed out that it appears that the cross-axis sensitivity and misalignment effects do contribute to the recorded strong-motion accelerations in an amount which is significantly larger than the overall amplitudes of digitization and processing noise whenever input accelerations approach the level of about 1 g. Typically, however, these effects do not seem to exceed more than 5 per cent of the input peak accelerations for the instrument type considered and as such may not be of concern for the majority of routine earthquake engineering applications.

Acknowledgments

We thank J. G. Anderson, D. E. Hudson, and W. Rihn for critical reading of the manuscript and for many useful comments and discussions.

This research was supported in part by grants from the National Science Foundation, by contracts from the U.S. Geological Survey and the Nuclear Regulatory Commission, and by the Earthquake Research Affiliates Program while the authors were at the California Institute of Technology. The work was completed at the University of Southern California with the support from the Nuclear Regulatory Commission and the National Science Foundation.

References

Anderson, J. A. and H. O. Wood (1925). Description and theory of the torsion seismometer, *Bull. Seism. Soc. Am.* **15**, 1–72.

Benioff, H. (1955). Earthquake seismographs and associated instruments, in *Advances in Geophysics*, vol. 2, H. E. Landsberg, Editor, Academic Press, New York.

Byerly, P. (1953). Theory of the hinged seismometer with support in general motion. *Bull. Seism. Soc. Am.* **43**, 251–261.

Dielman, R. J., T. C. Hanks, and M. D. Trifunac (1975). An array of strong-motion accelerographs in Bear Valley, California, *Bull. Seism. Soc. Am.* **65**, 1–12.

Rogers, P. W. (1968). The response of the horizontal pendulum seismometer to Rayleigh and Love waves, tilt, and free oscillations of the Earth, *Bull. Seism. Soc. Am.* **58**, 1384–1406.

Rogers, P. W. (1975). A note on the nonlinear response of pendulous accelerometer, *Bull. Seism. Soc. Am.* **65**, 523–530.

Skinner, R. L. and W. R. Stephenson (1973). Accelerograph calibration and accelerogram correction, *J. Earthquake Eng. Struct. Dyn.* **2**, 71–86.

Trifunac, M. D. (1971). Zero base-line correction of strong-motion accelerograms, *Bull Seism. Soc. Am.* **61**, 1201–1211.

Trifunac, M. D. (1972). A note on correction of strong-motion accelerograms for instrument response, *Bull. Seism. Soc. Am.* **62**, 401–409.

Trifunac, M. D. and D. E. Hudson (1970). Laboratory Evaluation and Instrument Corrections of Strong-motion Accelerographs, Earthquake Eng. Res. Lab., *Report No. EERL 70-04*, Calif. Inst. of Tech., Pasadena.

Trifunac, M. D. and V. W. Lee (1973). Routine Computer Processing of Strong-Motion Accelerograms, Earthquake Eng. Res. Lab., *Report No. EERL 73-03*, Calif. Inst. of Tech., Pasadena.

Trifunac, M. D., F. E. Udwadia, and A. G. Brady (1973). Analysis of errors in digitized strong-motion accelerograms, *Bull. Seism. Soc. Am.* **63**, 157–187.

Department of Civil Engineering
University of Southern California
Los Angeles, California 90007

Manuscript received August 17, 1976